

Lawrence Berkeley National Laboratory

Lawrence Berkeley National Laboratory

Title

THE EFFECTS OF AIR MELTING ON Fe/0.3C/ 3Cr/0.5Mo/2Mn AND Fe/0.3C/3Cr/0.5Mo/2Ni STRUCTURAL ALLOY STEELS

Permalink

<https://escholarship.org/uc/item/5n50j7gp>

Author

Steinberg, B.

Publication Date

1979-06-01

Peer reviewed

MASTER

LBL-9103



Lawrence Berkeley Laboratory

UNIVERSITY OF CALIFORNIA, BERKELEY, CA

Materials & Molecular Research Division

THE EFFECTS OF AIR MELTING ON Fe/0.3C/3Cr/0.5Mo/2Mn
AND Fe/0.3C/3Cr/0.5Mo/2Ni STRUCTURAL ALLOY STEELS

Beverlee Steinberg
(M. S. thesis)

June 1979



Prepared for the U. S. Department of Energy
under Contract W-7405-ENG-48

DISTRIBUTION OF THIS DOCUMENT IS UNLIMITED
wom

THE EFFECTS OF AIR MELTING ON Fe/0.3C/3Cr/0.5Mo/2Mn
AND Fe/0.3C/3Cr/0.5Mo/2Ni STRUCTURAL ALLOY STEELS

Contents

ABSTRACT	v
I. INTRODUCTION	1
II. EXPERIMENTAL PROCEDURE	4
A. Material Preparation.	4
B. Heat Treatment.	4
C. Mechanical Testing.	5
1. Tensile Testing	5
2. Charpy Impact Testing	5
3. Fracture Toughness.	5
4. Dilatometry.	5
D. Metallography	6
1. Optical	6
2. Fractography.	6
3. Electron Microscopy	6
III. RESULTS	8
A. Mechanical Properties	8
B. Fractography.	9
C. Microstructure.	11

NOTICE
This report was prepared as an account of work sponsored by the United States Government. Neither the United States nor the United States Department of Energy, nor any of their employees, nor any of their contractors, subcontractors, or their employees, makes any warranty, express or implied, or assumes any legal liability or responsibility for the accuracy, completeness, or usefulness of any information, apparatus, product, or process disclosed, or represents that its use would not infringe privately owned rights.

IV. DISCUSSION	13
V. CONCLUSIONS.	16
ACKNOWLEDGMENTS	17
REFERENCES	18
TABLES	21
FIGURE CAPTIONS	24
FIGURES	26

THE EFFECTS OF AIR MELTING ON Fe/0.3C/3Cr/0.5Mo/2Mn
AND Fe/0.3C/3Cr/0.5Mo/2Ni STRUCTURAL ALLOY STEELS

Beverlee Gail Steinberg

Materials and Molecular Research Division
Lawrence Berkeley Laboratory
and
Department of Materials Science and Mineral Engineering
University of California, Berkeley, California 94720

ABSTRACT

Changing production methods of a steel from vacuum melting to air melting can cause an increase in secondary particles, such as oxides and nitrides, which may have detrimental effects on the mechanical properties and microstructure of the alloy. In the present study a base alloy of Fe/0.3C/3Cr/0.5Mo with either 2Mn or 2Ni added was produced by air melting and its mechanical properties and microstructure were compared to an identical vacuum melted steel. Significant differences in mechanical behavior, morphology, and volume fraction of undissolved inclusions have been observed as a function of composition following air melting. For the alloy containing manganese, all properties remained very close to vacuum melted values but the 2Ni alloy displayed a marked loss in Charpy impact toughness and plane strain fracture toughness. This loss is attributed to an increase in volume fraction of secondary particles in the nickel alloy, as opposed to both the

manganese alloy and vacuum melted alloys, as well as to substantially increased incidence of linear coalescence of voids. Microstructural features are also discussed.

I. INTRODUCTION

When developing new alloys it has been found advantageous to work with vacuum melted materials in order to maintain a high purity product (1, 2, 3). In this way the effects of impurities, oxygen and nitrogen especially, are minimized and it may be assumed that all mechanical and microstructural properties can be attributed to the different alloying elements alone. For the past several years a research program at the University of California, Berkeley has aimed at developing structural alloy steels whose properties are to exceed those of the HSLA steels on the commercial market at comparably lower production costs. In order to study the effects of the different alloying additions and heat treatments by themselves, all work to date has involved vacuum melted steels.⁽⁴⁻¹³⁾

The purpose of the present investigation has been to determine the effects of air melting practices upon the already proven mechanical and microstructural properties of an Fe/0.3C/4Cr base alloy.⁽⁴⁻¹²⁾ The alloys were changed only slightly in this study to Fe/0.3C/3Cr/0.5Mo with either 2Mn or 2Ni added. The reasons for the alloying additions have been studied in much detail⁽⁴⁻¹³⁾ and will not be gone into again here.

The design properties desired in these steels are those of high strength and high toughness. It has been shown by Rao, et al.⁽⁷⁻¹¹⁾ that a microstructure of dislocated martensite laths surrounded

by thin, continuous films of stable retained austenite produces a material with excellent strength-toughness combinations. The high toughness is attributed to the austenite films while the dislocated martensite maintains the strength.

When a steel is air melted, or melted in a furnace open to the atmosphere, there is found to be a loss in ductility, dependent upon the melting atmospheric pressure. This effect decreases with increasing carbon content. The decrease in ductility in plain carbon steels is at a rate such that the difference between vacuum melting and air melting is found to be negligible at approximately 0.1 w/o carbon.⁽³⁾ Since the steels being studied have a carbon content of 0.3 w/o, it would appear to the first approximation that the effects of air melting will not be serious.

However, a major concern of air melting of alloy steels is that it will cause a substantial increase in oxides and nitrides. Ductility and toughness has been shown to decrease with increasing volume percent of secondary particles.^(3,14,15) This may be evidenced in a loss of toughness which is undesirable in these steels.

Voids may nucleate at second-phase particles either by cracking of the particle or by decohesion of the metal-particle interface. Growth and coalescence of voids follow. It is known that oxides crack while sulphides fail by decohesion. An increase in secondary particles could lead to early failure due to premature void coalescence brought about by decohesive or easily cracked particles. The size of particles is also important as it has been shown that coarser

inclusions fail at lower strain rates.⁽¹⁵⁾ On the other hand, with the presence of carbides the ductility may increase (or the effects of detrimental secondary particles may be offset) as the strain required for void nucleation increases with carbide percent. Carbides also do not crack or fail decohesively at low strain rates as compared to oxides or sulphides.⁽³⁾

In order to determine the effects of air melting practices, mechanical tests were performed and the alloys were examined microstructurally in scanning and transmission electron microscopes. The results will be used as part of the ongoing program to develop an economically attractive, high strength-high toughness structural steel. Comparisons will be made to similar vacuum melted alloys⁽¹⁵⁾ to determine changes in mechanical and microstructural properties. The heat treatment conditions of greatest interest are those which closely follow conventional commercial processes.

II. EXPERIMENTAL PROCEDURE

A. Material Preparation

The two alloys used were prepared and supplied courtesy of the Daido Steel Company of Japan and had the following design compositions (by weight percent): Fe/0.3C/3Cr/0.5Mo/2Mn, designated alloy 05; and Fe/0.3C/3Cr/0.5Mo/2Ni, designated alloy 08. The materials arrived in the form of 0.6 inch diameter bars and 1 × 3 inch slabs. Both alloys were sandblasted to remove any oxide scale and then homogenized at 1200°C for 24 hours followed by furnace cooling. The compositions of the alloys after homogenization are listed in Table 1.

B. Heat Treatment

Tensile, Charpy v-notch, and K_{IC} fracture specimens were cut and machined to oversized dimensions and then austenitized in vertical tube furnaces under a continuous flow of argon gas to minimize decarburization. After austenitizing at 1100°C for one hour, the specimens were quenched into agitated oil held at room temperature. Tempering was done for one hour in salt pots maintained at one of the following temperatures: 200°C, 300°C, 400°C, 500°C, or 600°C, all followed by a room temperature water quench. Final machining to remove the decarburized layer was then performed under flood cooling.

C. Mechanical Testing

1. Tensile testing. Room temperature tests to determine strength and ductility were performed on standard ASTM tensile specimens of 0.25 inch diameter and 1.25 inch gage length, Fig. 1. A hydraulic MTS testing machine with a 300 kip capacity and an 0.04 inch/minute crosshead speed was used in performing the tests.

2. Charpy impact testing. Standard ASTM Charpy v-notch specimens were used to determine toughness and the DBTT of both alloys. Charpy impact tests were run at room temperature while the DBTT tests were run at -196°C, -96°C, -36°C, 0°C, 25°C, and 100°C. The DBTT was determined for the as-quenched condition.

3. Fracture toughness. Compact tension specimens were tested per ASTM STP E399-74. Dimensions were as shown in Fig. 1. All specimens tested had both thickness, B, and crack length, a, greater than $2.5(K_Q/\sigma_{ys})^2$. Fatigue cracking and testing were done in the hydraulic MTS testing machine described under tensile testing.

4. Dilatometry. Dilatometry tests were run to determine the martensite start, M_s , martensite finish, M_f , austenite start, A_s , and austenite finish, A_f , phase transformation temperatures of the two alloys, Table 2. Tests were run in a commercial dilatometer.

D. Metallography

1. Optical. Specimens for optical observation were cut from broken Charpy v-notch specimens and mounted in Koldmont. Grinding was done on water cooled 120 and 240 grit belt sanders with finer grinding being done on 240, 320, 400, and 600 grit silicon carbide papers. Polishing was done on a 1 μm diamond paste wheel with final polishing done on a microcloth impregnated with 0.05 μm Al_2O_3 mixed into a slurry. 2% Nital was used to reveal the microstructure and prior austenite grain boundaries.

2. Fractography. Fracture surfaces were cut away from the bulk specimens and then cleaned in acetone. An AMR scanning electron microscope with an Energy Dispersive Analysis of X-rays (EDAX) attachment was used to view the fracture surfaces and to determine particle compositions.

3. Electron Microscopy. Materials for making thin foils for transmission electron microscopy was obtained by cutting 20 mil slices from bulk materials which had been heat treated as specified previously. These slices were then cleaned to remove any oxide scale and thinned to approximately 5 mils in a 4% solution of HF in H_2O_2 held at room temperature. The resulting chemically thinned slices were spark cut to 3.0mm discs and then sanded to a thicknesses of 1.5-2.0 mils. Final polishing was done in a twin jet electro-polishing apparatus

with a room temperature electrolytic solution of 75 gm. CrO_3 , 400 ml. CH_3COOH , and 21 ml. distilled water until there was a hole at the disc center. Polishing voltage was 35-45 volts. The resultant thin foils were stored in ethyl alcohol and examined in JEM 7A and Philips EM 301 microscopes run at 100 kV.

III. RESULTS

The major areas of interest in all the results and their comparisons to equivalent vacuum melted steels are the as-quenched and 200°C temper conditions as these relate most closely to the conventional heat treatments used in industry. Also, from earlier work on similar steels, the highest strength-toughness combinations were obtained for these two treatments.

A. Mechanical Properties

Results of the mechanical tests are tabulated in Table 3 and Fig. 2 through Fig. 8. The tensile properties of both alloys were consistent with those of previous investigators' (4-12) and highly compatible with tests run on vacuum melted steels of the same composition (13) as can be seen in Figs. 2 and 3. It should be noted that the alloys in Fig. 3 (vacuum melted steels) are slightly lower in carbon content and hence the slight lowering in strength values. The effects of the loss of carbon from solid solution at 200°C is seen as the value for ultimate tensile strength drops rapidly from the as-quenched condition.

An ill effect of air melting is seen through the Charpy impact data, Fig. 4 and Fig. 5. It is observed that the 2Mn alloy behaves as may be expected from the data of previous investigators but there is a detrimental drop in the Charpy v-notch toughness of the 2Ni alloy. As can be seen from the comparative data (13) of Fig. 5, this loss in

toughness is most obvious in the as-quenched and 200°C temper conditions, which are the conditions of highest interest. Drops in toughness at 300°C and 400°C are attributed to tempered martensite embrittlement as described by Rao ⁽¹⁰⁾, Rao and Thomas ⁽¹¹⁾, and Thomas. ⁽¹⁷⁾ At 500°C there is seen the effects of the classical temper embrittlement in the 2Mn steel. These embrittling effects also seem to be enhanced in the 2Ni air melted steel, although not to as great an extent as in the manganese alloy.

Ductile brittle transition temperature tests of as-quenched specimens the results of a great loss in toughness properties in the 2Ni alloy as this metal never displays an upper shelf, Fig. 6. Also, reduction in area values, Fig. 7, show the 2Mn alloy in the 200°C temper condition to have up to 10% better reduction in area than the 2Ni steel in the same condition. Plane strain fracture toughness values also support this lowering of properties in the 2Ni alloy, Table 3.

B. Fractography

Fractographs of the alloys can be seen in Fig. 8 through Fig. 14. Examination of the fracture surfaces of the broken Charpy impact specimens revealed that the fracture modes of the two alloys differed greatly. The 2Mn specimens displayed transgranular fracture in the as-quenched; Fig. 8c,d; and 200°C temper; Fig. 9c,d; conditions. This changes to quasi-cleavage fracture in the 300°C, Fig. 10c, and 400°C, Fig. 10d, temper samples and becomes pure intergranular fracture in the 600°C temper specimens, Fig. 12c,d. The 2 Ni alloys fractured by

combinations of dimple fracture and quasi-cleavage mechanism throughout all tempering conditions, Figs. 8-14, a&b. The quasi-cleavage fracture would indicate particle cracking, hence a larger concentration of oxides.

The nickel containing steels also exhibited a higher density of particles than the manganese containing alloys. Ductility decreases with secondary particle volume per cent (3,14,15) as void formation, growth, and coalescence begins around particles. It has also been shown by Cox and Low (15) that particle size plays an important role as the larger particles fracture or initiate voids first at lower strains with smaller and smaller inclusions failing as the strain increases. All this can lead to premature void coalescence occurring before the true toughness potential in the nickel alloy can be reached; for example, see the reduction in area, Fig. 7.

Another phenomenon seen is the presence of long "striations" of rib-like fractures in all tempering ranges of the nickel alloy, Fig. 14. These fractures average approximately 15-20 μm in length with the ribs inside fairly evenly spaced at 1-1.5 μm . These fractures are not found in the 2Mn specimens. Too large to be interlath paths and not following any set direction, it is concluded that these rib-like fractures are caused by linear coalescence of voids, which may be an end result of linear conglomeration of oxides, and are themselves a weaker fracture path helping to bring about premature fracture.

The particles found in the samples proved to be MnS, Al₂O₃, and combinations thereof, Fig. 13. Particles of (Fe,Mn)S were also found. Although oxides containing Mn or Ni may be found, it is difficult to identify them with the x-ray analysis of the EDAX attachment. However, as can be seen in Table 4, the free energies of formation of oxides and nitrides of manganese and nickel support the probability of their presence. It should be noted that the values of Gibb's Free Energy are given in the table for both room temperature and T > 1550°C and that the more negative the free energy, the more likely for the oxide or nitride to be present.

C. Microstructure

The morphology of both alloys at all tempering temperatures was dislocated lath martensite as described by Das and Thomas⁽²¹⁾, Thomas⁽²²⁾, and Thomas and Rao.⁽²³⁾ In the as-quenched and 200°C temper conditions these martensite laths were surrounded by nearly continuous films of retained austenite, Fig. 15 and Fig. 16, although these austenite films were substantially harder to find in the nickel containing alloy. The retained austenite films were neither as continuous nor as thin as might be expected from comparisons with previous work.^(5-11,17) The average film thickness seen is approximately 0.04 μm. Analysis of the selected area diffraction patterns revealed that the relationships between the retained austenite and martensite are those of Kurdjumov-Sachs, i.e.:

$$(011)_M // (111)_\gamma$$

$$[\bar{1}\bar{1}\bar{1}]_M // [\bar{1}10]_\gamma$$

and Nishiyama-Wasserman, i.e:

$$(011)_M // (111)_\gamma$$

$$[100]_M // [10\bar{1}]_\gamma.$$

Retained austenite has not been found in the 300°C temper condition, Figs. 17-18. This lack of retained austenite is a cause for the enhanced effect of temper martensite embrittlement seen in the mechanical properties as discussed by earlier investigators. (19,11,17)

In the lower tempering conditions, Widmanstätten carbides could be seen as shown in Fig. 16c where the carbides are visible in the bright field. The nickel containing alloys displayed ϵ -carbides in the lower tempering conditions. As tempering temperatures increased, small carbides, found to be cementite, were seen to be evenly dispersed throughout the martensite laths; Figs. 19,20; although some carbides were seen between laths. The carbides and cementite were rod shaped with the cementite having a length of roughly 200 Å.

IV. DISCUSSION

When the alloy containing manganese is air melted, little or no change is seen in the mechanical properties while the alloy containing nickel experiences a marked drop in toughness and ductility. Fracture surfaces reveal that there is an increase in the amount of second-phase particles within the 2Ni steel as compared to the 2Mn alloy. This effect is most obviously seen in the fractographs of the alloys in the as-quenched and 200°C temper conditions, Figs. 8 and 9. The particles ranged in size, on an average, from 0.2 μm to 3 μm with the average dimple diameter approximately 10 times the particle size. It could be estimated that the volume percent of particles in the nickel alloy is roughly 10 times that of the particles in the manganese alloy. The inter-particle spacing in the nickel alloy is roughly 5-10 μm while the spacing between the particles in the 2Mn alloy is approximately 15-20 μm . It has been shown ^(3,14) that ductility decreases exponentially with amount of secondary particles. Since void nucleation, coalescence, and growth takes place around particles, the 2Ni alloy could be fracturing prematurely at all tempering temperatures due to the increase in particles. However, since the nickel containing steel also failed by quasi-cleavage, there must be particle cracking or the presence of oxides.

Another feature seen in the SEM fractographs is the existence of rib-like fractures in all tempering ranges of the nickel steel, Fig. 14. These fracture modes are not seen in the manganese alloy and may

be attributed to linear coalescence of voids causes a weaker fracture path once again aiding in premature fracture.

From the Charpy v-notch toughness curves, Figs. 4 and 5, it is seen that there is a drastic drop in toughness of the 2Mn alloy at the 300°C tempering condition. This loss in toughness can be attributed to the loss of retained austenite in the microstructure. Conversion of the interlath austenite to carbides causes fracture paths to prefer interlath routes, a phenomenon called temper martensite embrittlement and studied by Rao ⁽¹⁰⁾, Rao and Thomas ⁽¹¹⁾, and Thomas. ⁽¹⁷⁾ This has been shown to be a direct cause of lower toughness in steels. The nickel alloys also suffer from temper martensite embrittlement at this stage but the effect is not as obvious due to their already low toughness state and perhaps more thermal stability in retained austenite. ⁽¹⁰⁾

Another cause of the lower toughness in the nickel alloy may be attributed to the amount of retained austenite present. Although it is difficult to determine quantitatively the actual amounts of retained austenite in the nickel alloy than in the manganese alloy. Thus, if the austenite stabilizing elements are locked up in carbides and secondary inclusions they obviously do not have as much an effect on stabilizing austenite in the material upon quenching. Since the presence of retained austenite is a predominate factor in obtaining high toughness, its reduction is an obvious further cause in lowering the mechanical properties.

Due to the inadequacies of the EDAX attachment on the SEM it is not possible to obtain detailed particle analysis and effects of air

melting on chemical composition across laths and around particles. It would be advantageous to look at alloys in STEM or Auger to see if these effects could be determined. In this way it may be found that the causes of the lowering of mechanical properties in the nickel steel are also due to chemical problems encountered in the melting process.

V. CONCLUSIONS

1. The air melting of an Fe/0.3C/3Cr/0.5Mo/2Mn alloy does not greatly affect the mechanical properties or microstructure as compared to a similar vacuum melted steel and hence this less expensive production process can be used with great success.
2. There are detrimental effects on the mechanical properties of an Fe/0.3C/3Cr/0.5Mo/2Ni alloy when it is produced by air melting. The greatest losses are in the Charpy impact toughness and fracture toughness properties. Increased amounts of intermetallic particles in the alloy, linear coalescence of voids, and smaller amounts of interlath retained austenite films are the main causes of these losses in mechanical properties.
3. Classical temper embrittlement around 500°C tempering appears to be enhanced by air melting in the 2Mn modified alloy.

ACKNOWLEDGMENTS

The author would like to express her appreciation to Professor Gareth Thomas and Dr. B. V. N. Rao whose patience and guidance supported her throughout the research. She would also like to thank Carolyn Gosnell whose friendliness, supreme patience and knowledge of the microscope keeps everyone going day to day and Mehmet Sarikaya who so graciously allowed her the use of his vacuum melted data as a comparison.

Thanks are also due to Professors Iain Finnie and J. W. Morris, Jr. for their review of this manuscript.

The author wishes to thank the technical support staff of the Materials and Molecular Research Division for all their help in machining and in performing of mechanical tests.

Special thanks are extended to my parents, Gabe and Gerry Steinberg, who supported me along my chosen path and especially to my husband, Chad Alexander, who showed a rare love and patience which kept me going while we remained apart.

This work was supported by the Division of Basic Energy Sciences, United States Department of Energy under Contract No. W-7405-Eng-48 through the Materials and Molecular Research Division of the Lawrence Berkeley Laboratory.

REFERENCES

1. W. H. Wills, Jr., Metal Progress, Nov. 1967, 60.
2. M. B. Balakhovskaya, N. A. Khusainova, and L. N. Davlyatova, Steel in the USSR, Dec. 1975, 685.
3. F. B. Pickering, Toward Improved Ductility and Toughness, Conference of Iron and Steel Institute of Japan, Oct. 1971, 9.
4. J. A. McMahon, M. S. Thesis, University of California, Lawrence Berkeley Laboratory Report, LBL-1181 (1973).
5. B. V. N. Rao and G. Thomas, Materials Science and Engineering, 20 (1975), 195.
6. J. A. McMahon and G. Thomas, Microstructure and Design of Alloys, Proc. Int. Conf. Strength of Materials (1972), 180.
7. B. V. N. Rao, M. S. Thesis, University of California, Lawrence Berkeley Laboratory Report LBL-3794 (1975).
8. B. V. N. Rao, R. W. Miller, G. Thomas, "Heat Treatment '76," Proc. 16th Int. Heat Treat. Conf., England, May 1976.
9. M. F. Carlson, B. V. N. Rao, R. O. Ritchie, G. Thomas, Paper presented at the 4th Int. Conf. Strength of Materials and Alloys, Nanch, France, Aug. 1976, LBL-5111.
10. B. V. N. Rao, Ph.D. Thesis, University of California, Lawrence Berkeley Laboratory Report LBL-7361 (1978).
11. B. V. N. Rao and G. Thomas, Paper submitted to Met. Trans., Lawrence Berkeley Laboratory Preprint LBL-8064 (1978).
12. M. Carlson, M. S. Thesis, University of California, Lawrence Berkeley Laboratory Report LBL-7670 (1978).

13. M. Sarikaya, unpublished data.
14. 'Effect of Second-Phase Particles on the Mechanical Properties of Steel', Iron and Steel Inst., London, 1971.
15. T. B. Cox and J. R. Low, Jr., Met. Trans. 5, June 1974, 1457.
16. B. V. N. Rao, J. Y. Koo, and G. Thomas, 33rd Ann. Proc. Electron Microscopy Soc. Amer., Nevada 1975.
17. G. Thomas, Met. Trans. A 9A, March 1978, 439.
18. S. K. Das and G. Thomas, Met. Trans. 1, Jan. 1970, 325.
19. G. Thomas, 'Fundamental Aspects of Structural Alloy Design', Plenum Pub. Corp., N. Y., 331 (1977).
20. B. V. N. Rao, Paper prepared for the National Science Foundation, Lawrence Berkeley Laboratory Report LBL-8013 (1978).
21. S. K. Das and G. Thomas, ASM 62, 659 (1969).
22. G. Thomas, Met. Trans. 2, Sept. 1971, 2373.
23. G. Thomas and B. V. N. Rao, Pres. at the Int. Conf. on Martensite Trans., Kiev, USSR, 1977, LBL-6242.
24. J. R. Low, Jr., D. F. Stein, A. M. Turkalo, and R. P. LaForce, Trans. AIME 242, Jan. 1968, 14.
25. 'ASM Metals Handbook', 9.
26. 'CRC Handbook of Chemistry and Physics', 55th ed.
27. R. M. Horn and R. O. Ritchie, Met. Trans. A 9A, Aug. 1978, 1039.
28. E. C. Bain, 'Alloying Elements in Steel', ASM Ohio, 1961.
29. R. W. K. Honeycombe, 'Structure and Strength of Alloy Steels.'
30. R. Kiessling and N. Lange, 'Non-Metallic Inclusions in Steel', Iron and Steel Inst., London, 1964.

31. H. J. Schrader, *Stal in English*, June 1969 (6), 470.
32. G. R. Speich and W. C. Leslie, *Met. Trans.* 3, May 1972, 1043.
33. R. O. Ritchie and R. M. Horn, *Met. Trans. A* 9A, March 1978, 331.
34. Y. L. Chen, PhD. Thesis, University of California, Lawrence Berkeley Laboratory Report LBL-5423 (1976).
35. J. Chipman, *Met. Trans.* 3, Jan. 1972, 55.
36. J. S. Pascover and S. V. Radcliffe, *Trans. AIME* 242, 1968, 673.
37. P. M. Kelly, J. Nutting, *Journal of Iron and Steel*, March 1961, 199.
38. S. V. Zagulyaeva and M. I. Vinograd, Central Scientific-Research Inst. of Ferrous MET., July 1977.
39. R. A. Grange, *Met. Trans.* 2, Jan. 1971, 65.
40. K. J. Irvine, F. B. Pickering, and J. Garstone, *Journal of Iron and Steel*, Sept. 1960, 66.
41. I. Cheng and G. Thomas, *Met. Trans.* 3, Feb. 1972, 503.
42. J. D. Bolton, E. R. Petty, and G. B. Allen, *Met. Trans.* 2, Oct. 1971, 2915.
43. F. Habrovec, J. Skarek, and P. Rys. *Mat. Sci. and Eng.* 21, (1975), 93.
44. W. W. Gerberich, P. L. Hemmings, and V. F. Zackay, *Met. Trans.* 2, Aug. 1971, 2243.
45. M. Raghavan and G. Thomas, *Met. Trans.* 2, Dec. 1971, 3433.
46. E. R. Parker, *Met. Trans. A* 8A, (7) July 1977, 1055.
47. R. D. Garwood and G. Thomas, *Met. Trans.* 4, 1973, 225.

TABLE 1. Weight percent chemical composition after homogenization.

<u>ALLOY</u>	<u>C</u>	<u>Cr</u>	<u>Mo</u>	<u>Mn</u>	<u>Ni</u>	<u>Si</u>	<u>P</u>	<u>S</u>	<u>Cu</u>	<u>Al</u>
2Mn	.29	2.94	.52	1.86	.03	.01	.017	.009	.02	.042
2Ni	.30	3.19	.48	.10	2.11	.15	.007	.012	.01	.047

TABLE 2. Transformation temperatures and grain sizes.

<u>ALLOY</u>	<u>M_s</u>	<u>M_f</u>	<u>A_s</u>	<u>A_f</u>	<u>Grain size</u>
	<u>°C</u>	<u>°C</u>	<u>°C</u>	<u>°C</u>	
2Mn	330	220	750	780	320
2Ni	320	195	750	780	250

TABLE 3. Mechanical properties.

Alloy	Tempering temperature °C	YS (KSI)	UTS (KSI)	% Reduction in area	% Elongation total (uniform)	K _{IC} KSI-IN ^{1/2}	Charpy v-notch energy (ft-lbs)
2Mn	As-quenched	189.6	263	14.08	6.43 (3.86)	104.0	29.75
	200 ^p	196.3	238	26.5	7.35 (4.32)	117.3	39.93
	300	183.8	222.8	25.58	6.24 (2.88)		14.93
	400	181.3	213.2	16.33	6.72 (3.28)		13.33
	500	168.2	200.7	27.01	9.04 (4.24)		10.55
	600	135	153.8	46.20	12.80 (4.40)		14.00
2Ni	As-quenched	206.5	270.4	16.68	7.22 (4.00)	69.1	13.75
	200	202.3	250.6	19.02	13.65 (3.92)	84.8	22.5
	300	186.4	224.6	19.02	9.59 (2.96)		21.75
	400	180.8	215.4	15.38	10.50 (3.52)		21.25
	500	171.1	205.0	30.13	14.17 (4.24)		23.88
	600	140.0	160.4	43.76	18.68 (4.32)		47.75

TABLE 4. Heats of formation and free energies for some inclusions (26).

T = 25°C			T > 1550°C		
Inclusion	ΔH° kcal/g m	ΔG° kcal/g m	Inclusion	ΔH_o kcal/g m	ΔG_t kcal/g m
Al ₂ O ₃	-399.09	-376.77	Al ₂ O ₃	-407.95	-260.50
MnO	- 92.0	- 86.8	MnO	- 93.35	- 13.13
Cr ₂ O ₃	-263.7	-250.2	Cr ₂ O ₃	-278.03	-158.99
Fe ₃ O ₄	-267.0	-242.4	Fe ₃ O ₄	-257.24	-130.38
NiO	- 58.4	- 51.7	NiO	- 58.83	- 14.79
Fe ₂ O ₃	-196.50	-177.1	Fe ₂ O ₃	These form below 1550°C	
MnO ₂	-124.5	-111.4	MnO ₂		
Mn ₂ O ₃	-232.1	---	Mn ₂ O ₃		
Mn ₃ O ₄	-331.4	-306.0	Mn ₃ O ₄		
AlN	- 57.7	- 50.1			
Al ₂ S ₃	-121.6	-117.7			
CrN	- 29.8	---			
Cr ₂ N	- 23.4	---			
FeS	- 22.77	- 23.32			
Mn(N ₃) ₂	92.2	---			
Mn ₅ N ₂	- 57.8	---			
Mn ₈ N ₂	- 81.0	---			
Mn(NO ₃) ₂	-166.32	---			
Mns	- 48.8	- 49.9			
NiS	- 17.5	---			
Ni(NO ₃) ₂	-102.2	---			

FIGURE CAPTIONS

- Figure 1. Final dimensions of tensile, plane strain fracture toughness, and Charpy v-notch toughness specimens.
- Figure 2. Ultimate tensile and yield strength as a function of tempering temperature, air melted alloys.
- Figure 3. Ultimate tensile and yield strengths as a function of tempering temperature, vacuum melted steels. Note the carbon w/o is 0.05 lower than desired.
- Figure 4. Charpy impact toughness as a function of tempering temperature, air melted alloys.
- Figure 5. A comparison of Charpy impact toughness values for air and vacuum melted steels.
- Figure 6. Ductile Brittle Transition Temperature curves, air melted alloys.
- Figure 7. Reduction in Area and Total Elongation of air melted alloy as a function of tempering temperature.
- Figure 8. Fractographs of alloys in the as-quenched condition:
(a) 2Ni, 500X; (b) 2Ni, 2000X; (c) 2Mn, 500X,
(d) 2Mn, 2000X.
- Figure 9. Fractographs of alloys in the 200°C temper condition:
(a) 2Ni, 500X; (b) 2Ni 2000X; (c) 2Mn, 200X; (d) 2Mn,
2000X.
- Figure 10. Fractographs of alloys in the 300°C temper and
400°C temper conditions: (a) 2Ni, 300°C temper, 500X;

(b) 2Ni, 400°C temper, 500X; (c) 2Mn, 300°C temper, 100X;
(d) 2Mn, 400°C temper, 100X.

Figure 11. Fractographs of alloys in the 500°C temper condition:

(a) 2Ni, 500X; (b)-(d) 2Mn, 50X, 500X, 200X respectively.

Figure 12. Fractographs of alloys in the 600°C temper condition:

(a) 2Ni, 500X; (b) 2Ni, 2000X; (c) 2Mn, 50X; (d) 2Mn, 200X.

Figure 13. Fractographs showing particle analysis. Particles shown are

MnS. (a) 2Ni, 5000X; (b) 2Mn, 2000X.

Figure 14. Fractograph showing rib-like fractures in the nickel steel, see arrows. These fractures are caused by linear coalescence of voids. 300°C temper.

Figure 15. Bright field and dark field micrographs showing retained austenite in the 2Mn alloy, as-quenched condition, 25k mag.

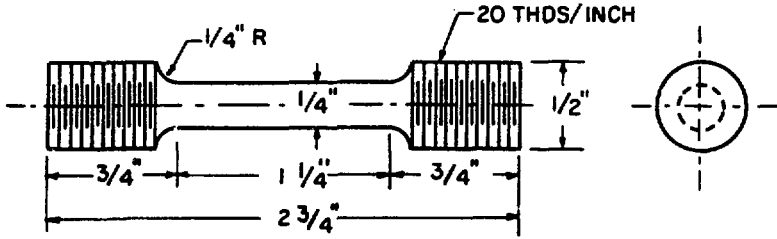
Figure 16. Micrographs showing retained austenite in 200°C tempered alloys: (a) and (b) 2Mn, 25k mag; (c) and (d) 2Ni, 25k mag.

Figure 17. Bright and dark field micrographs showing $[01\bar{1}]$ carbides in the 2Mn alloy in the 300°C temper condition, 30k mag.

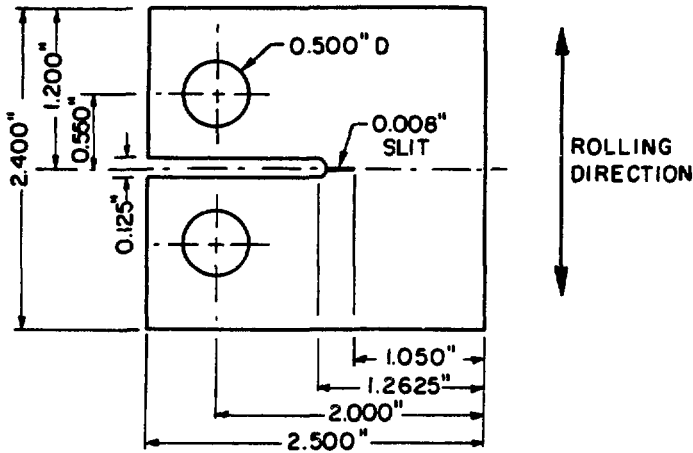
Figure 18. Carbides in the 2Ni alloy, 300°C temper condition, 40k mag.

Figure 19. Cementite in the 2Mn, 400°C tempered alloy, 36k mag.

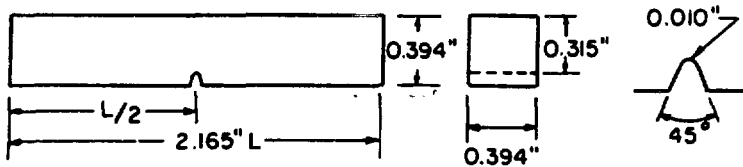
Figure 20. Carbides in the 2Ni, 400°C tempered alloy, 35k mag.



A. ROUND TENSILE SPECIMEN



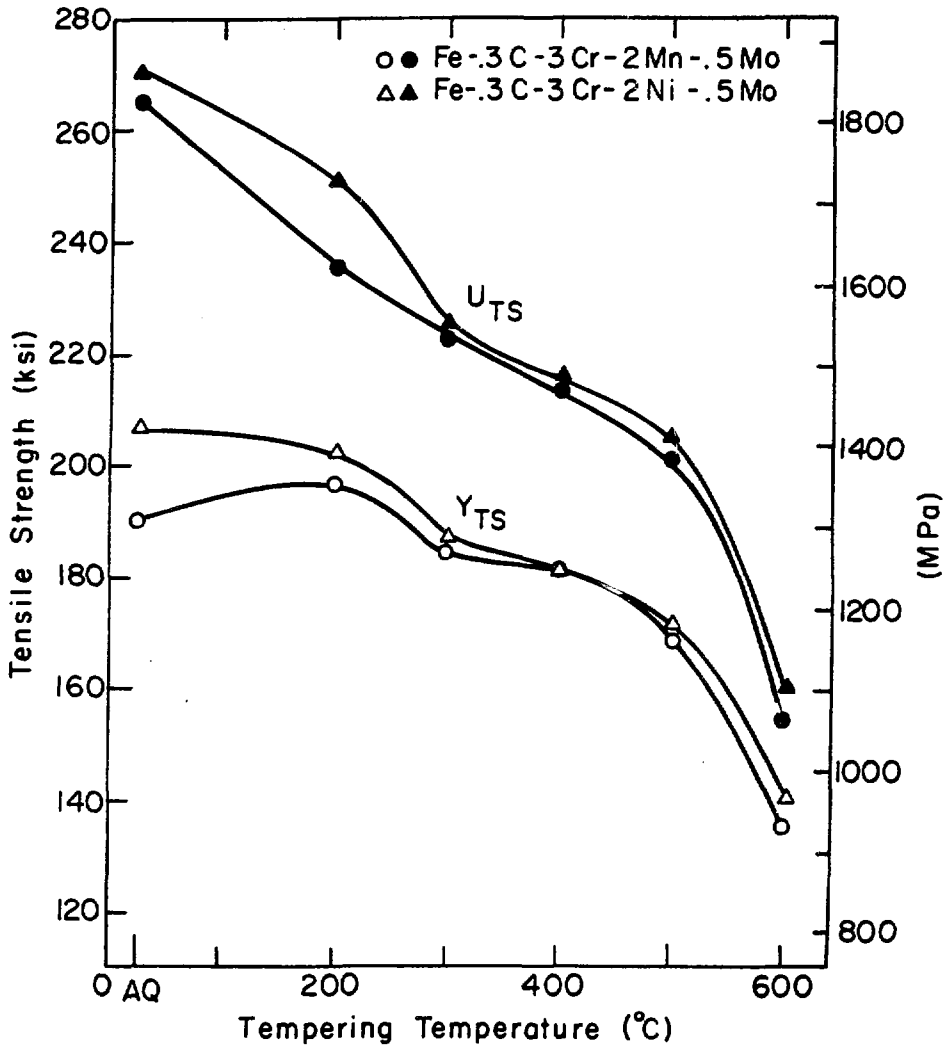
B. FRACTURE TOUGHNESS SPECIMEN



C. CHARPY V-NOTCH IMPACT SPECIMEN

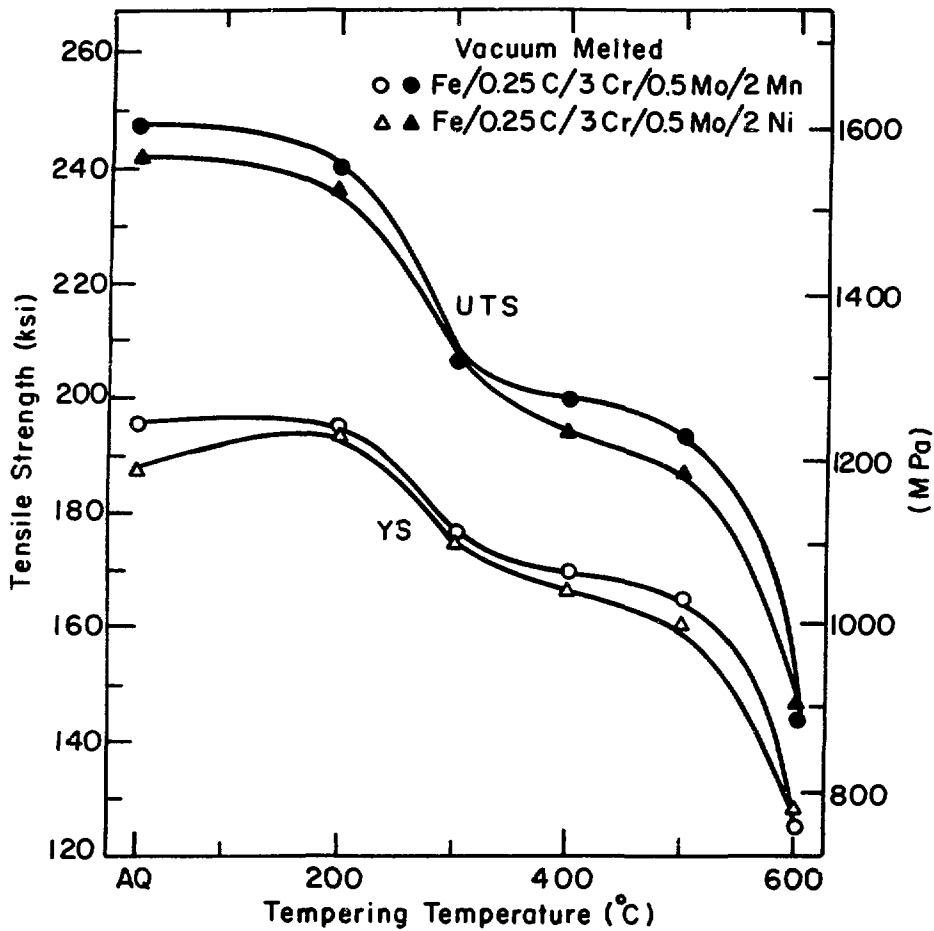
XBL 754-6176

Figure 1



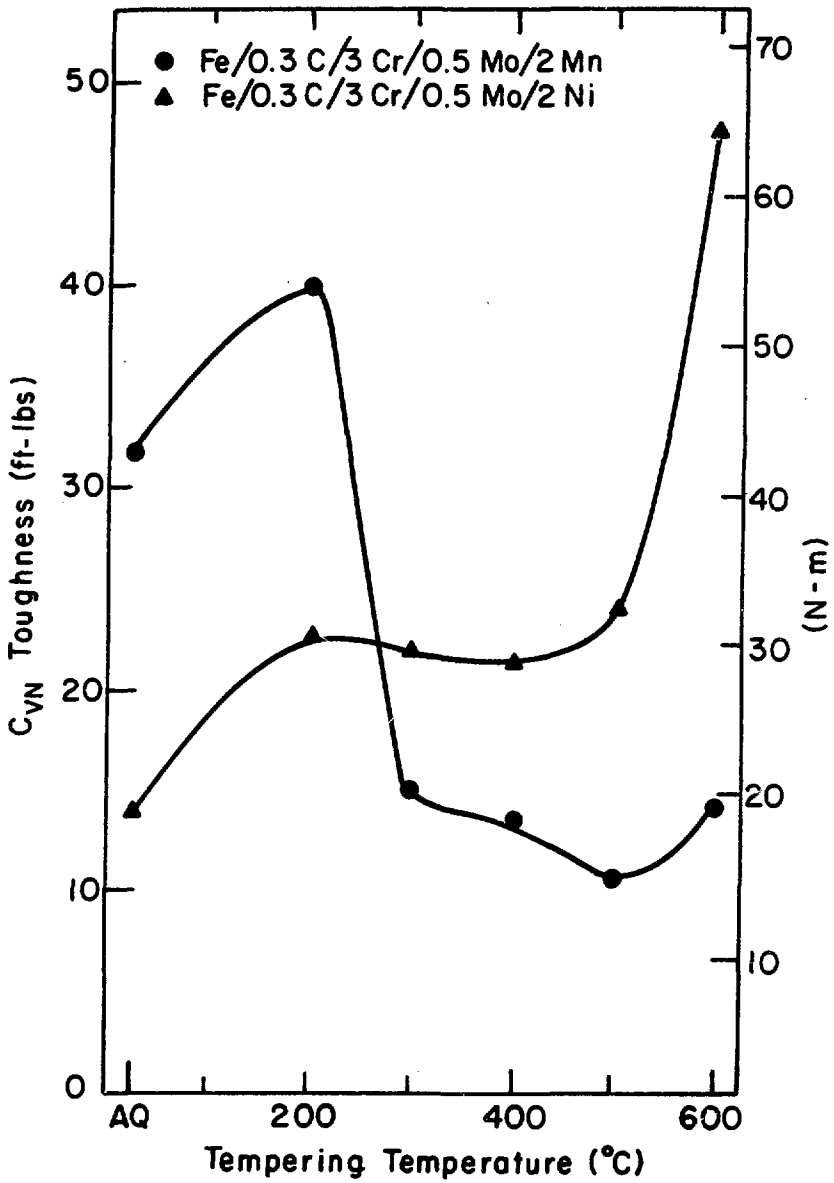
XBL7811-6145

Figure 2



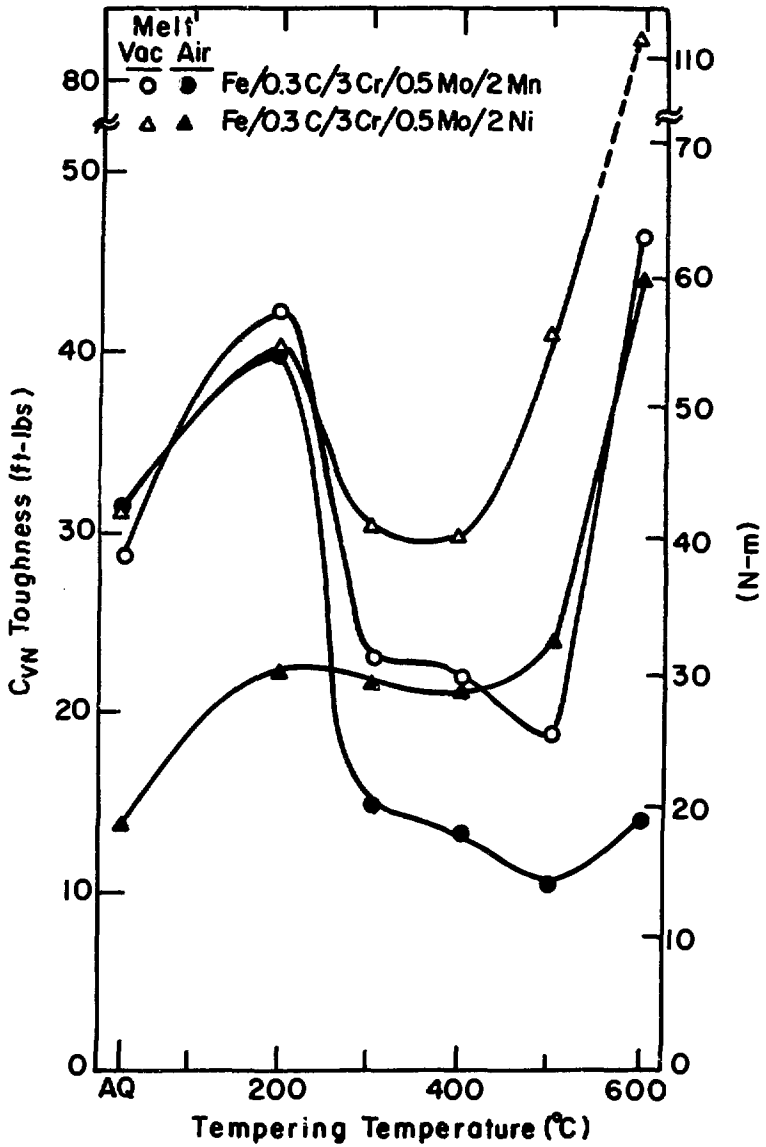
XBL 79 3-5966

Figure 3



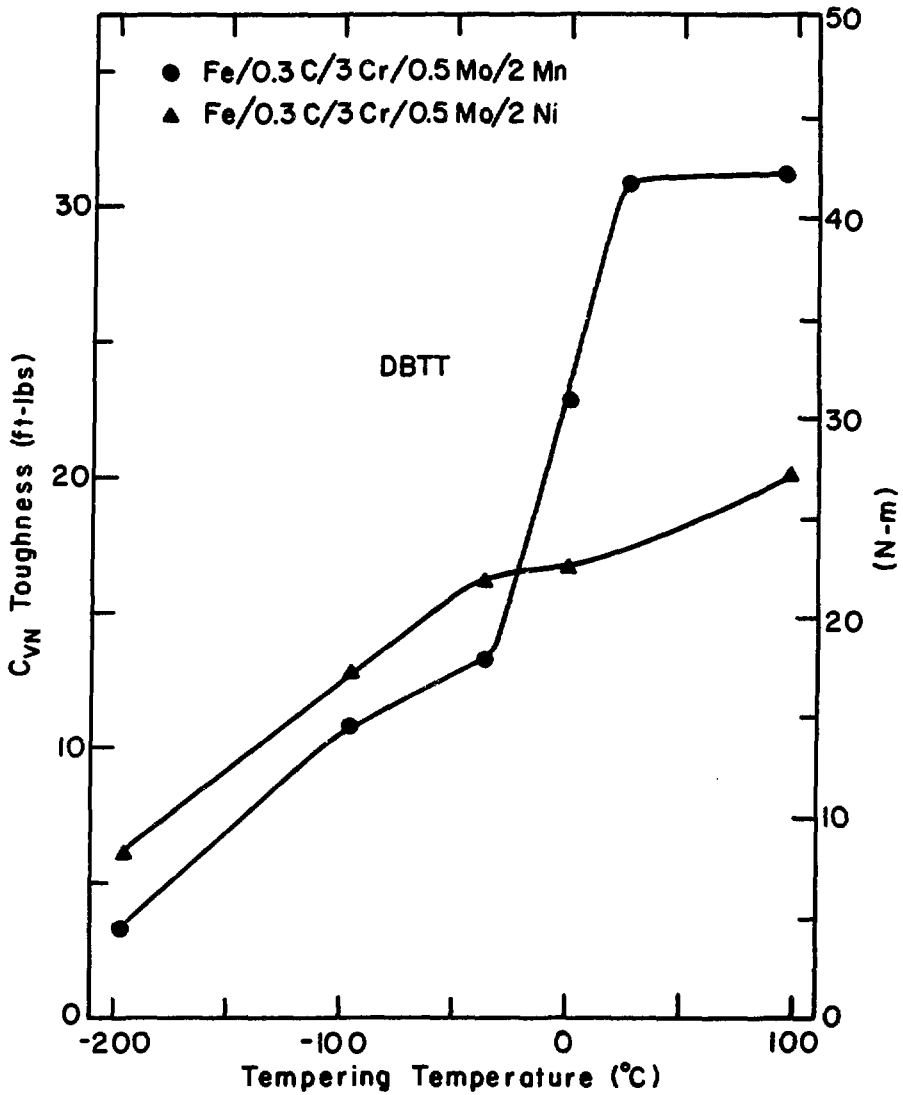
XBL 793-5963

Figure 4



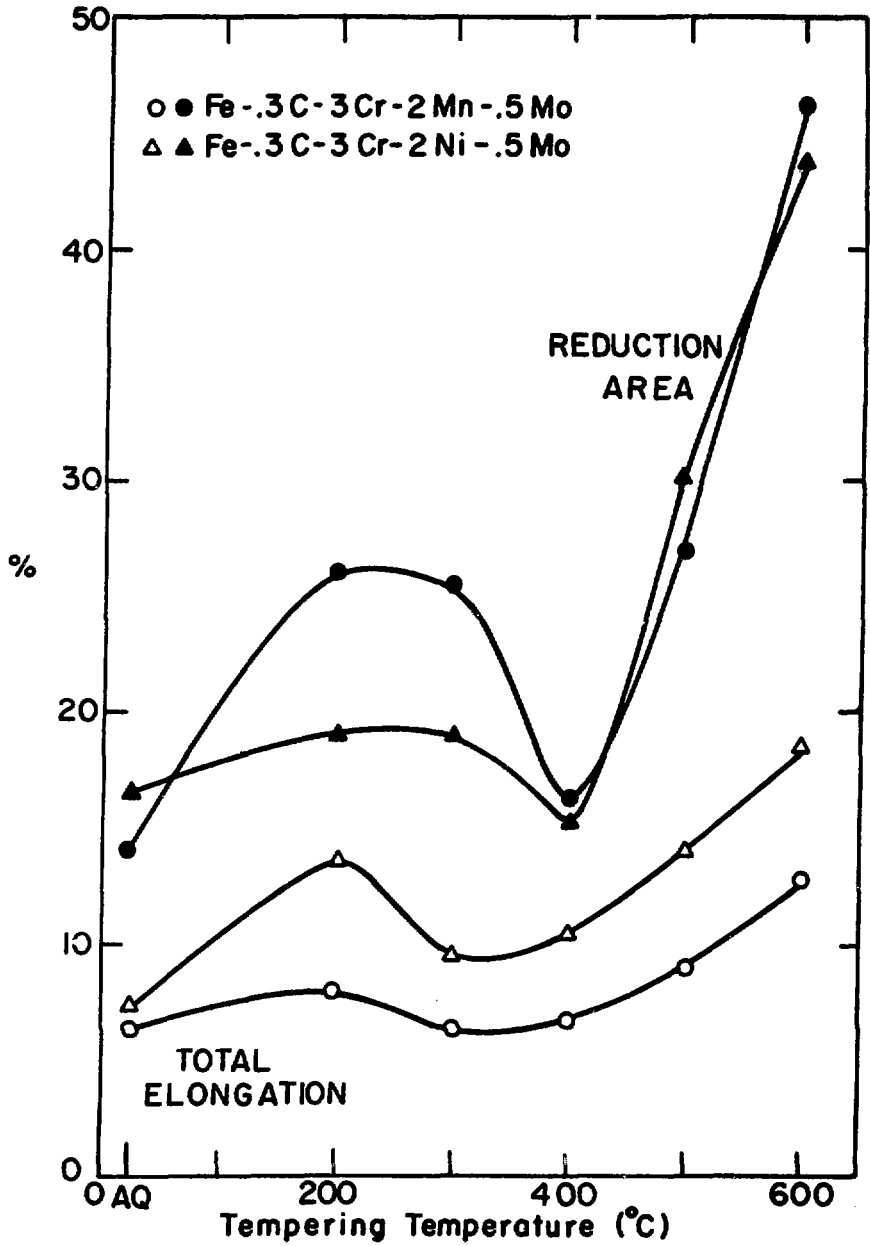
XBL 793-5965

Figure 5



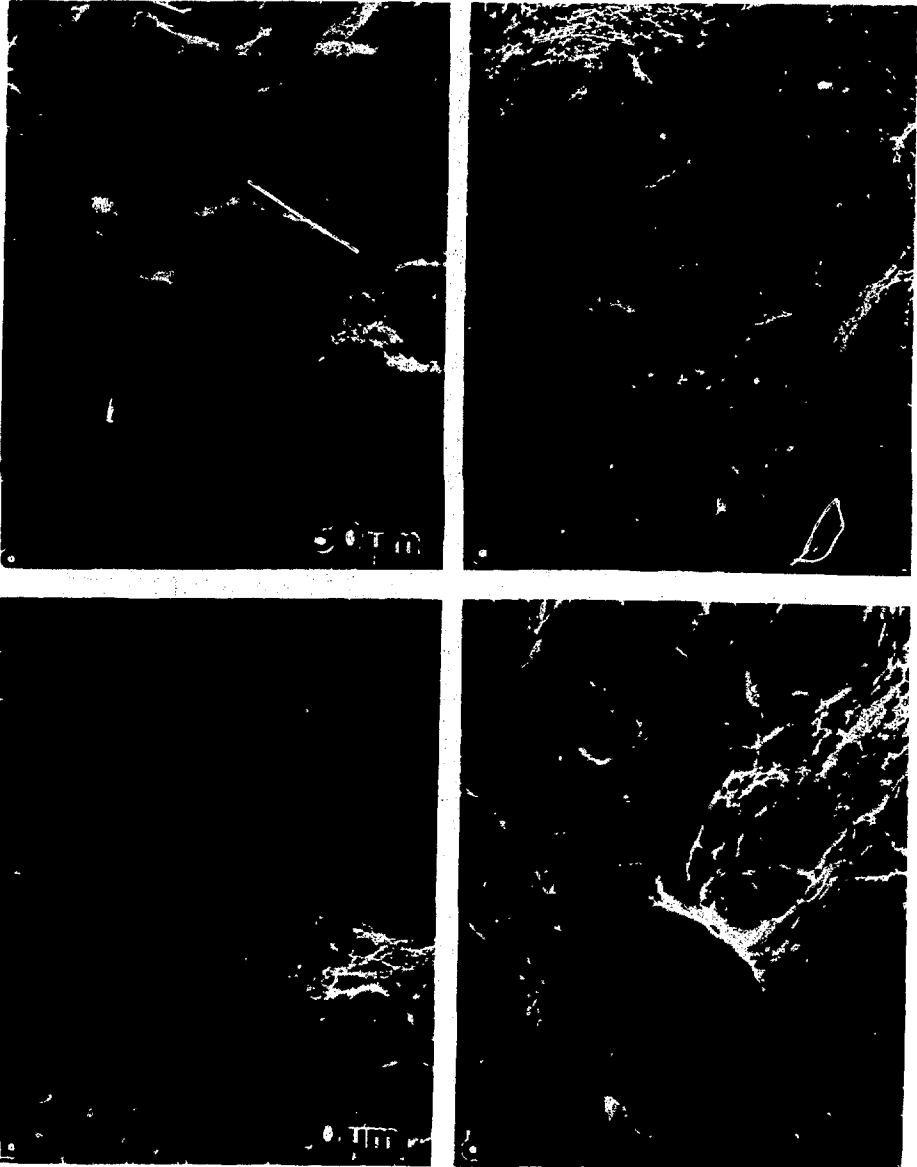
XBL793-5964

Figure 6



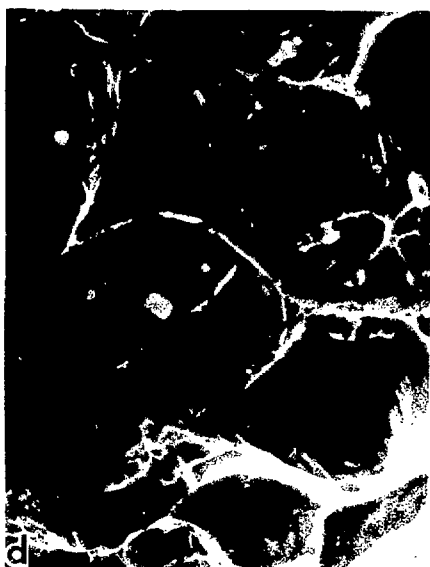
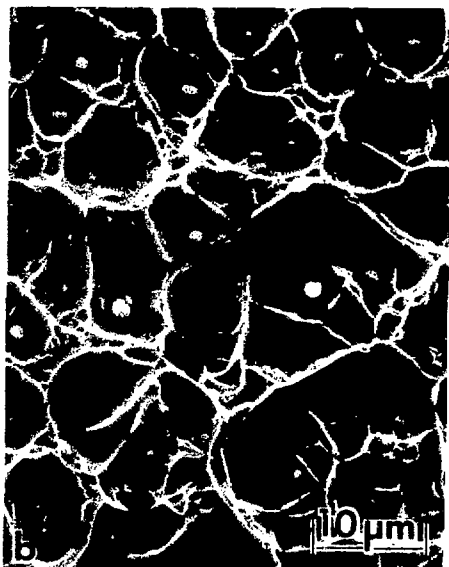
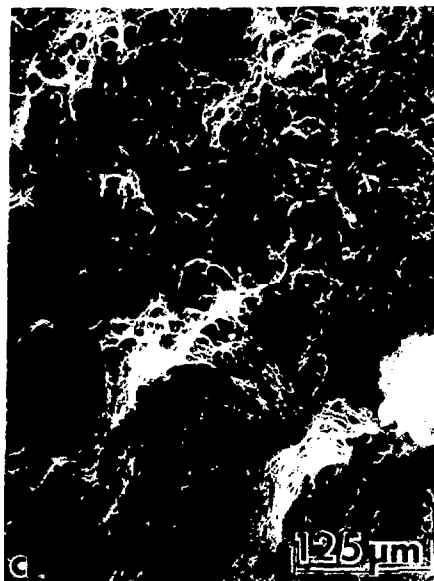
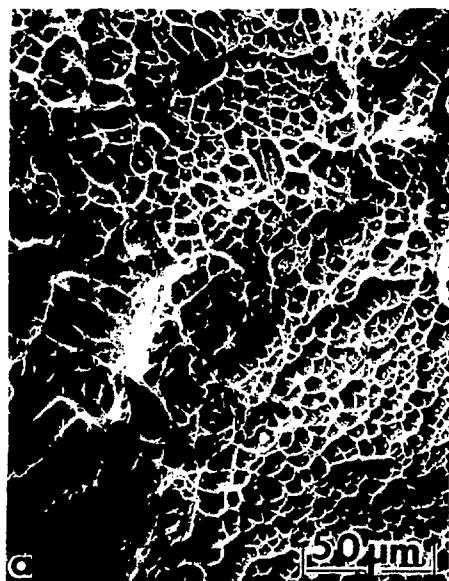
XBL 7811-6144

Figure 7



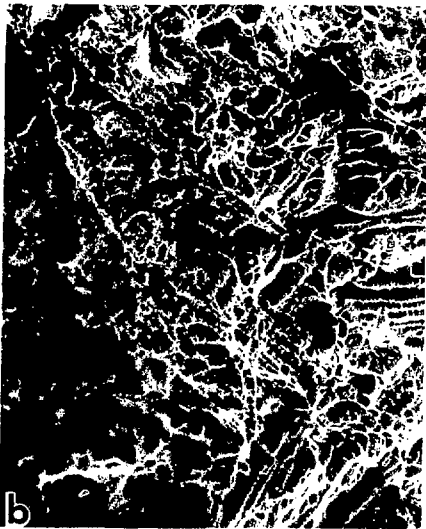
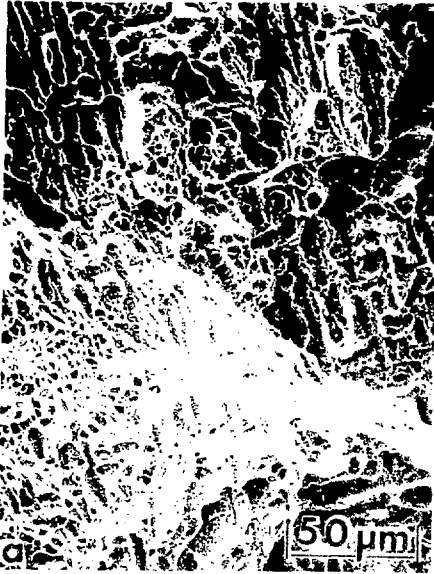
XBB 780-14420

Figure 8

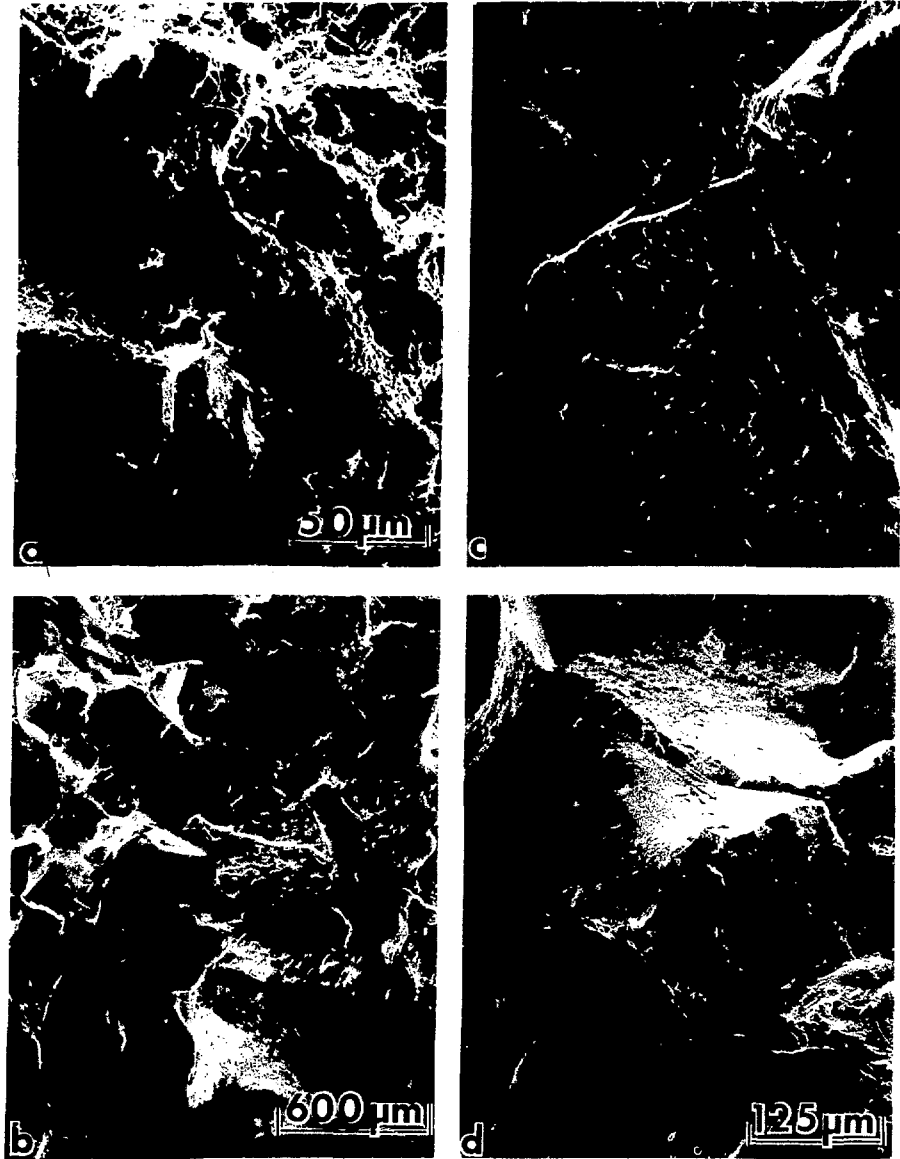


100000x

Figure

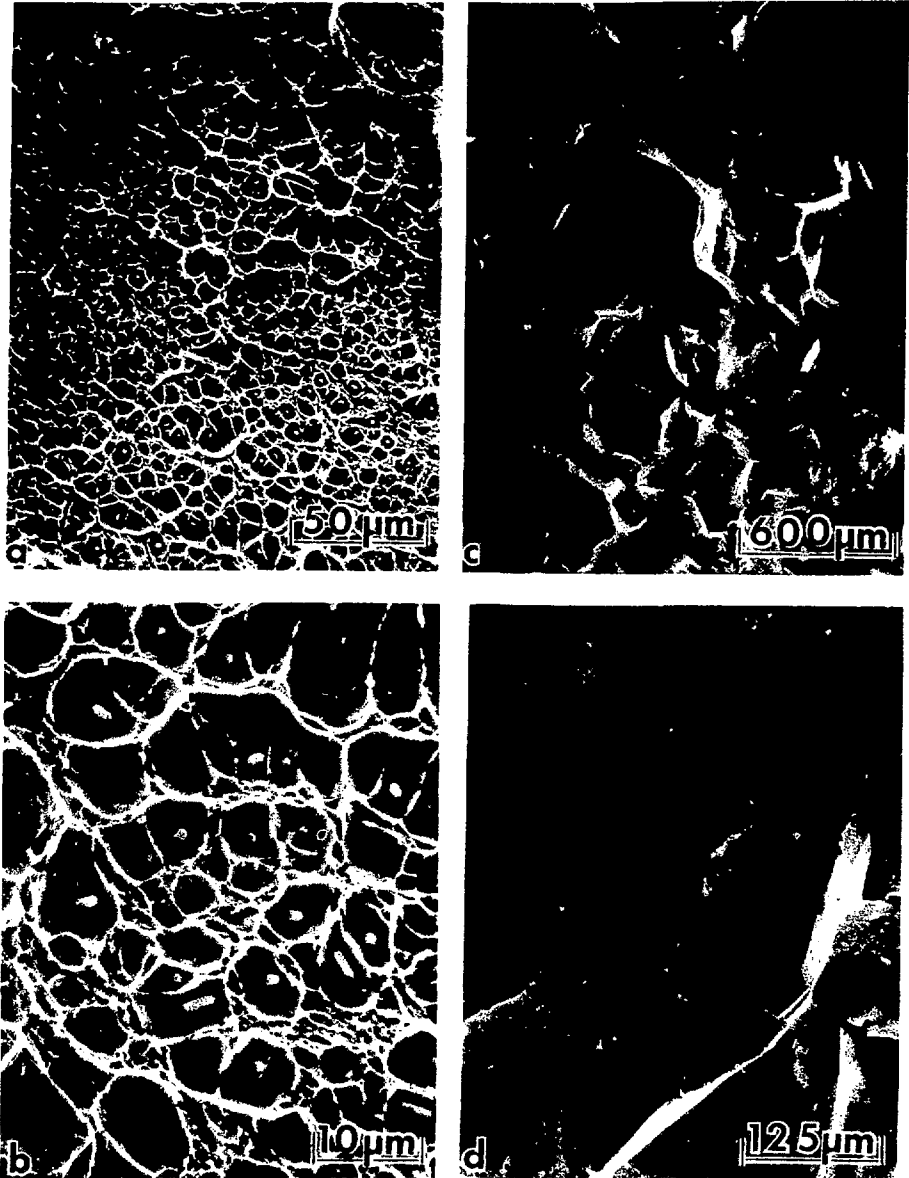


33-795-5504



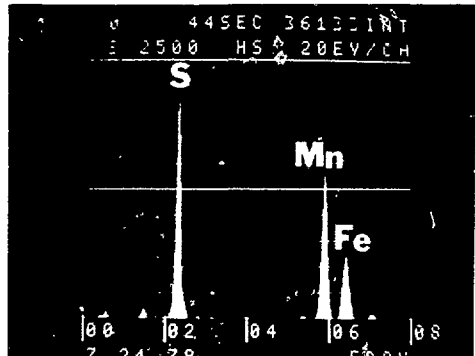
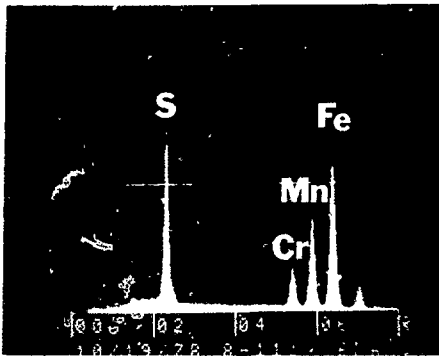
XBB 780-14418

Figure 11



NBB 780-14417

Figure 12



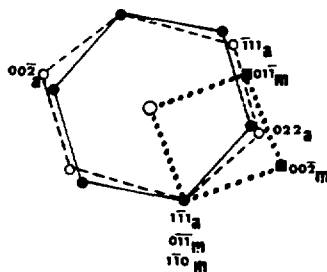
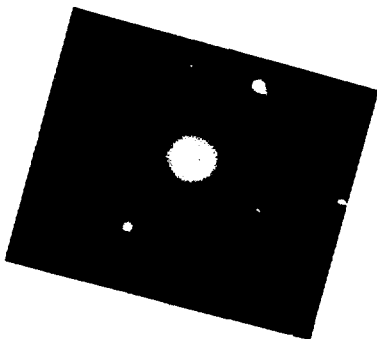
NBB 795-5809

Figure 17



Figure 11

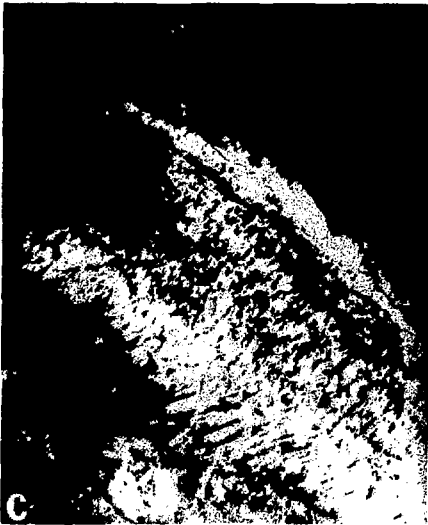
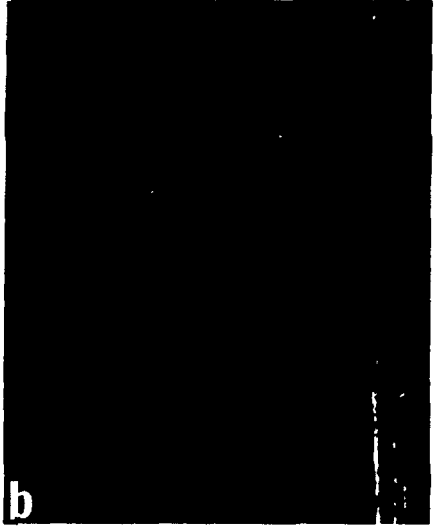
100000-200000



— $[1\bar{1}0]$ MARTENSITE
- - - $[00\bar{2}]$ MARTENSITE
- - - $[1\bar{1}0]$ AUSTENITE

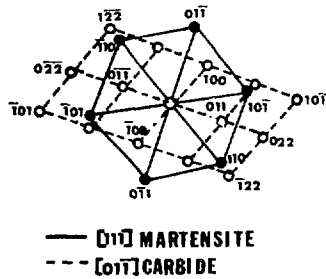
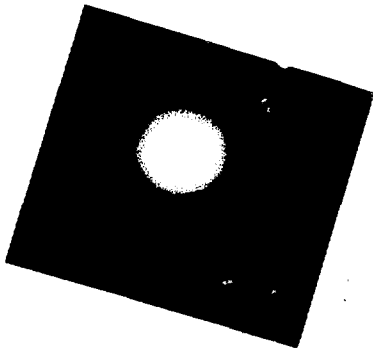
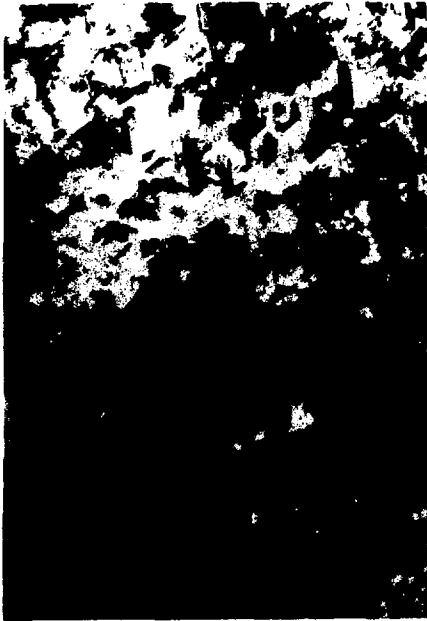
XBB 793-3312

Figure 15



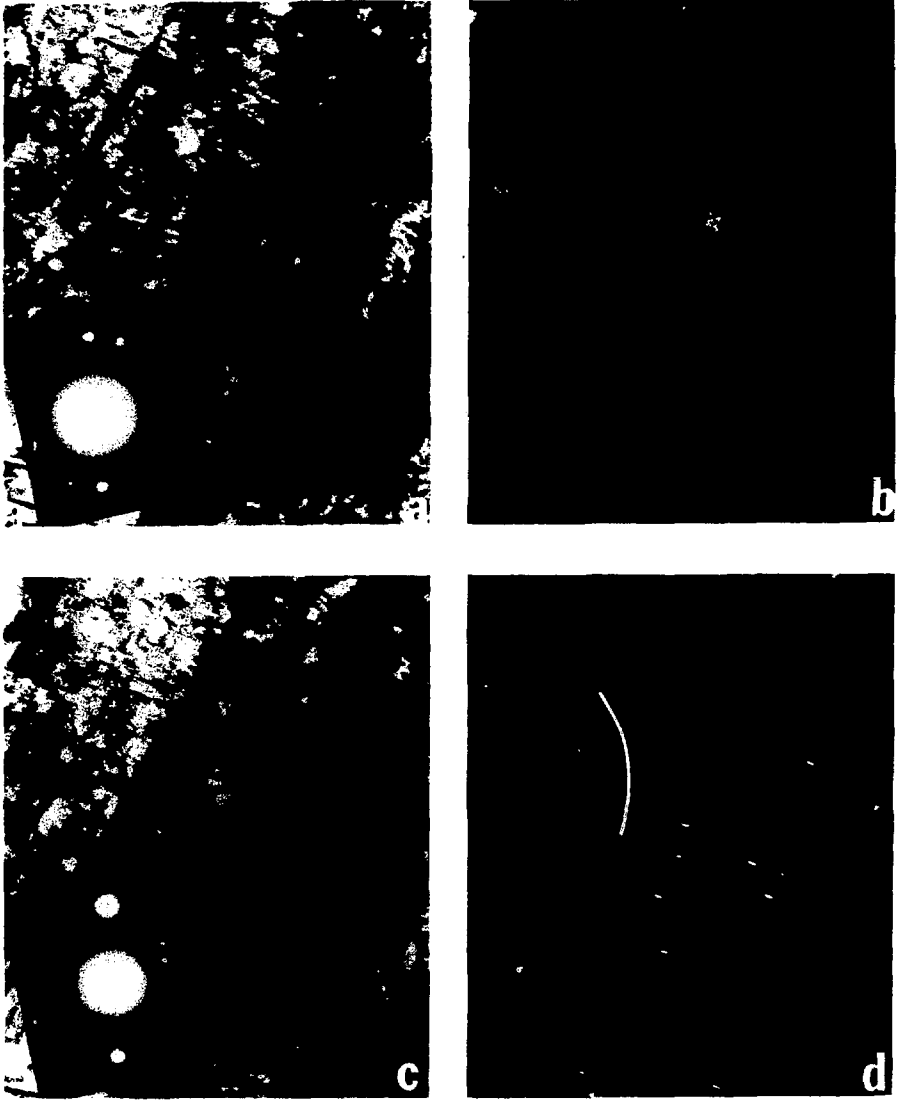
XBB 793-3305

Figure 16



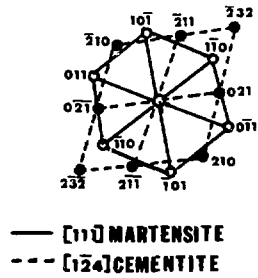
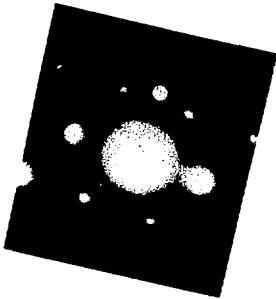
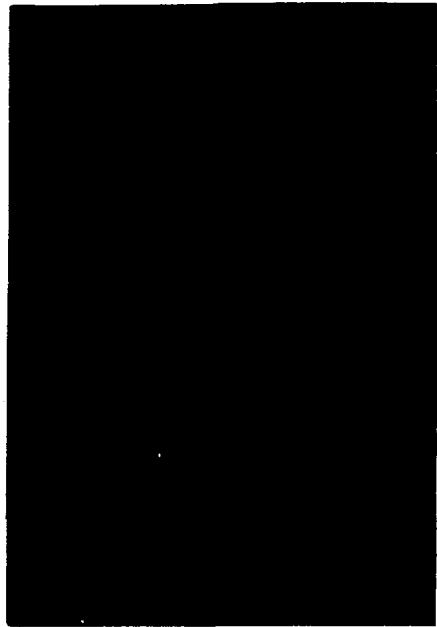
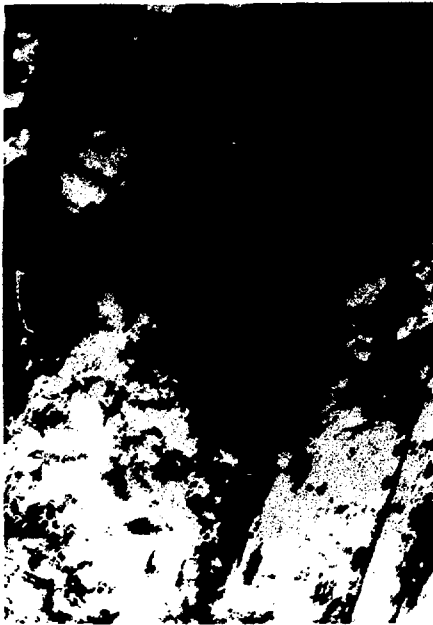
XBB 793-3311

Figure 17



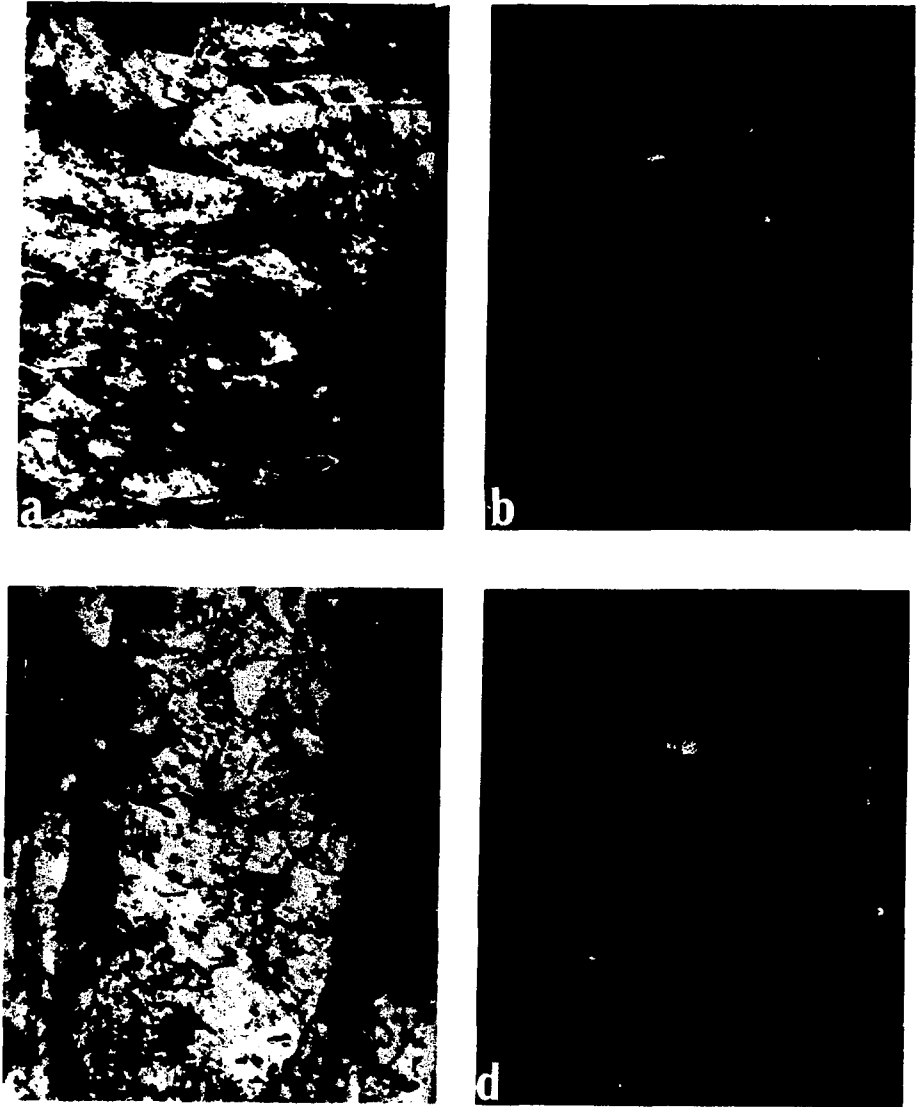
XBB 793-3307

Figure 18



XBB 793-3310

Figure 19



XBB 793-3306

Figure 20